ACCOUNTS
of chemical research

A Hybrid Atomistic Electrodynamics–Quantum Mechanical Approach for Simulating Surface-Enhanced Raman Scattering

JOHN L. PAYTON, SETH M. MORTON, JUSTIN E. MOORE, AND LASSE JENSEN*

Department of Chemistry, The Pennsylvania State University, 104 Chemistry Building, University Park, Pennsylvania 16802, United States

RECEIVED ON MARCH 15, 2013

CONSPECTUS

Surface-enhanced Raman scattering (SERS) is a technique that has broad implications for biological and chemical sensing applications by providing the ability to simultaneously detect and identify a single molecule. The Raman scattering of molecules adsorbed on metal nanoparticles can be enhanced by many orders of magnitude. These enhancements stem from a twofold mechanism: an electromagnetic mechanism (EM), which is due to the enhanced local field near the metal surface, and a chemical mechanism (CM), which is due to the adsorbate specific interactions between the metal surface and the molecules. The local field near the metal surface can be significantly enhanced due to the plasmon excitation, and therefore chemists generally accept that the EM provides the majority of the enhancements.

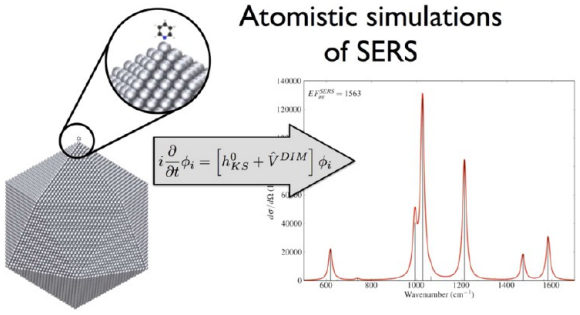

While classical electrodynamics simulations can accurately simulate the local electric field around metal nanoparticles, they offer few insights into the spectral changes that occur in SERS. First-principles simulations can directly predict the Raman spectrum but are limited to small metal clusters and therefore are often used for understanding the CM. Thus, there is a need for developing new methods that bridge the electrodynamics simulations of the metal nanoparticle and the first-principles simulations of the molecule to facilitate direct simulations of SERS spectra.

In this Account, we discuss our recent work on developing a hybrid atomistic electrodynamics–quantum mechanical approach to simulate SERS. This hybrid method is called the discrete interaction model/quantum mechanics (DIM/QM) method and consists of an atomistic electrodynamics model of the metal nanoparticle and a time-dependent density functional theory (TDDFT) description of the molecule. In contrast to most previous work, the DIM/QM method enables us to retain a detailed atomistic structure of the nanoparticle and provides a natural bridge between the electronic structure methods and the macroscopic electrodynamics description.

Using the DIM/QM method, we have examined in detail the importance of the local environment on molecular excitation energies, enhanced molecular absorption, and SERS. Our results show that the molecular properties are strongly dependent not only on the distance of the molecule from the metal nanoparticle but also on its orientation relative to the nanoparticle and the specific local environment. Using DIM/QM to simulate SERS, we show that there is a significant dependence on the adsorption site. Furthermore, we present a detailed comparison between enhancements obtained from DIM/QM simulations and those from classical electrodynamics simulations of the local field. While we find qualitative agreement, there are significant differences due to the neglect of specific molecule–metal interactions in the classical electrodynamics simulations. Our results highlight the importance of explicitly considering the specific local environment in simulations of molecule–plasmon coupling.

1. Introduction

Metal nanoparticles exhibit unique optical properties due to their ability to support surface plasmons. The coupling between molecules and plasmons leads to a wide range of optical phenomena such as surface-enhanced linear and nonlinear vibrational spectroscopy,[1,2] surface-enhanced fluorescence,[3,4] and plasmon–exciton hybridization.[5] This has led to many applications of plasmons in optics, in

Published on the Web 08/21/2013 www.pubs.acs.org/accounts
10.1021/ar400075r

catalysis, and as sensors for chemical and biological detection.[6] Thus, it is of fundamental importance to establish at a molecular level an understanding of the coupling between molecules and plasmons.

Surface-enhanced vibrational spectroscopies, such as surface-enhanced Raman scattering (SERS),[7−10] rely directly on the coupling between the molecule and the plasmon excitation. In SERS, the Raman scattering of adsorbed molecules can be enhanced by more than $\times 10^8$ such that a single molecule can be detected and identified due to the unique Raman fingerprint.[11−15] The SERS enhancement arises predominantly from the strong local field due to the plasmon excitation, the so-called electromagnetic mechanism (EM), and it be can shown that the Raman scattering scales as $\sim|E|^4$ where $|E|$ is the local field at the position of the molecule.[16−18] In addition to the EM, there is also an enhancement due to the short-range interactions between the metal and the molecule called the chemical mechanism (CM). The overlap between the wave functions of the molecule and the metal results in a renormalization of the molecular orbitals as well as the introduction of new mixed charge-transfer states; both of these effects will contribute to CM enhancement of the Raman signal.[8,19−21] While all of these mechanisms contribute to the observed enhancements, it is possible in some situations to separate the CM and EM mechanisms.[22] The different enhancement mechanisms can then be modeled separately and compared with experiments. Although we have a fairly well developed understanding of the enhancement mechanisms, we only have a rudimentary understanding of spectral changes that occur in SERS due to the complicated nature of the metal−molecule interface.[18,20] It remains a formidable challenge to simulate realistic SERS spectra from first-principles due to the complexity of correctly treating the interactions of an electronically localized molecular system with the electronically delocalized structure of a metal particle that is many nanometers in dimension.

Typically, the EM contribution to SERS is considered by simulating the local electric field due to the plasmon excitation using classical electrodynamics.[23] Several efficient approaches are available to simulate the optical properties of metal nanoparticles and have been shown to correlate with experimental results. However, recent work has highlighted the importance of quantum effects in junctions between metal nanoparticles with small gaps due to electron tunneling effects.[5] This work has shown that there is a quantum mechanical limit on the EM enhancements in SERS.[24] Furthermore, any microscopic detail of the coupling is neglected since the nanoparticle and the molecular layer are represented as continuous objects characterized by their frequency-dependent dielectric functions. Despite their success for modeling the optical properties of nanoparticles, this lack of microscopic detail prevents a realistic description of the molecule−metal interface and thus cannot provide a complete description of SERS. First-principles simulations offer a unique tool that can provide the detailed understanding of the complicated interface by directly simulating the SERS spectrum that can be compared with experiments.[18−20,25] However, due to large computational requirements, first-principles methods are limited to small systems and thus are typically used to provide information about the CM in SERS.[18−22,25] Therefore, it is necessary to develop new methods that bridge the quantum mechanical description of the molecule and the classical electrodynamics description of the metal nanoparticle to provide a comprehensive understanding of SERS.

In recent years, several different hybrid methods that combine a quantum mechanical description of the molecule and a classical description of the metal nanoparticle have emerged.[26−37] While these methods offer an improved quantum mechanical description of the molecule, the description of the metal nanoparticle is often based on a continuum treatment and thus neglects the relevant specific interactions. To overcome these limitations, our group has been developing an atomistic electrodynamics model[38,39] and combined it with time-dependent density functional theory (TDDFT).[40−42] This method, which we denote the discrete interaction model/quantum mechanics (DIM/QM) method, represents the nanoparticle atomistically, enabling the modeling of the influence of the local environment of a nanoparticle surface on the optical properties of a molecule. The DIM/QM method can be seen as an extension of traditional polarizable QM/MM methods used for describing optical properties of molecules in solution. In contrast to most previous work, the DIM/QM method enables us to retain the detailed atomistic structure of the nanoparticle and provides a natural bridge between the electronic structure methods and the macroscopic electrodynamics description.

In this Account, we will highlight our recent work on understanding the coupling between molecules and plasmons using the DIM/QM method. We will illustrate the importance of the local environment on molecular excitation energies, enhanced molecular absorption, and SERS. As a direct test of the well-known $|E|^4$ approximation for describing SERS enhancements, we will present a detailed comparison between enhancements obtained using the

DIM/QM method and those obtained using the EM approximation. Our results highlight the importance of explicitly considering the specific local environment in simulations of molecule−plasmon coupling and the need for directly simulating the SERS spectra.

2. An Atomistic Electrodynamics−Quantum Mechanical Approach

In the DIM/QM method, the nanoparticle is considered as a collection of N interacting atoms that describe the total optical response. For large metal nanoparticles, each atom is characterized by an atomic polarizability obtained from the experimental dielectric constant. For smaller metal nanoparticles, we describe each atom by an atomic polarizability and an atomic capacitance that is obtained by fitting against TDDFT results for small silver clusters ($N < 68$).[38,39] This allows us to include size-dependent effects and thus correctly describe the saturation of the polarizability of the nanoparticle as the size increases.

In the DIM/QM model, the total energy is given by[40−42]

$$U^{\mathrm{TOT}}[\rho] = T_s[\rho] + \frac{1}{2}\int\int \frac{\rho(r)\rho(r')}{|r - r'|}\,\mathrm{d}r\,\mathrm{d}r' + U_{\mathrm{xc}}[\rho] + \int \rho(r) V_{\mathrm{nuc}}(r)\,\mathrm{d}r + U^{\mathrm{DIM/QM}}[\rho] \quad (1)$$

with the individual terms being the kinetic energy of a fictitious noninteracting system, the Coulomb energy, the XC-energy (exchange correlation), the electron−nuclear interaction energy, and the interaction energy describing the molecule−metal interactions, respectively. The interaction energy is given by

$$U^{\mathrm{DIM/QM}}[\rho] = U^{\mathrm{POL}}[\rho] + U^{\mathrm{VDW}} \quad (2)$$

where $U^{\mathrm{POL}}[\rho]$ is the polarization energy (the energy required to induce the dipoles and charges in the DIM system) and U^{VDW} accounts for the dispersion and repulsion energy between the DIM and the QM system. U^{VDW} is treated purely classically and thus does not depend on the ground state density. The polarization energy for a neutral nanoparticle is given by

$$U^{\mathrm{POL}}[\rho] = \frac{1}{2}\sum_m^N q_m^{\mathrm{ind}}[\rho] V_m^{\mathrm{SCF}}[\rho] - \frac{1}{2}\sum_m^N \mu_{m,\alpha}^{\mathrm{ind}}[\rho] E_{m,\alpha}^{\mathrm{SCF}}[\rho] \quad (3)$$

where μ_m^{ind} and q_m^{ind} are the dipoles and charges induced in the DIM system by the QM system, and $E_{m,\alpha}^{\mathrm{SCF}}$ and V_m^{SCF} are the electric field and potential arising from the QM system. Variational minimization of the total energy given by eq 1 leads to the following effective Kohn−Sham operator, $h_{\mathrm{KS}}[\rho(\mathbf{r}_j)]$, given by

$$h_{\mathrm{KS}}[\rho(\mathbf{r}_j)] = -\frac{1}{2}\nabla^2 - \sum_j \frac{Z_j}{|\mathbf{r}_j - \mathbf{R}_j|} + \int \frac{\rho(\mathbf{r}_j)}{|\mathbf{r}_j - \mathbf{r}_i|}\,\mathrm{d}\mathbf{r}_i + \frac{\delta E^{\mathrm{XC}}}{\delta\rho(\mathbf{r}_j)} + \hat{V}^{\mathrm{dim}}(\mathbf{r}_j) \quad (4)$$

with the individual terms being the kinetic energy, the nuclear potential, the Coulomb potential, the XC-potential, and the embedding DIM operator ($\hat{V}^{\mathrm{DIM}}(\mathbf{r}_j)$) describing the molecule−metal interactions, respectively. The embedding operator is given by

$$\hat{V}^{\mathrm{DIM}}(\mathbf{r}_j) = \sum_m \frac{q_m^{\mathrm{ind}}}{|\mathbf{r}_{jm}|} - \sum_m \frac{\mu_{m,\alpha}^{\mathrm{ind}} r_{jm,\alpha}}{|\mathbf{r}_{jm}|^3}. \quad (5)$$

The perturbation to the density due to the $\hat{V}^{\mathrm{DIM}}(\mathbf{r}_j)$ operator can be thought of as the image field, that is, the field arising from the dipoles and charges that are induced in the nanoparticle (DIM system) by the presence of the molecule (QM system). The interactions are damped at short distances to avoid over polarization.

The induced dipoles and charges needed to calculate the polarization energy are found by solving a set of $4N + 1$ linear equations expressed in supermatrix notation as

$$\begin{pmatrix} \mathbf{A} & -\mathbf{M} & 0 \\ -\mathbf{M}^{\mathrm{T}} & -\mathbf{C} & 1 \\ 0 & 1 & 0 \end{pmatrix} \begin{pmatrix} \mu^{\mathrm{ind}} \\ q^{\mathrm{ind}} \\ \lambda \end{pmatrix} = \begin{pmatrix} \mathbf{E}^{\mathrm{SCF}} \\ \mathbf{V}^{\mathrm{SCF}} \\ q^{\mathrm{DIM}} \end{pmatrix} \quad (6)$$

where the matrix **A** describes the dipole−dipole interactions, the matrix **M** describes interactions between dipoles and charges, and the matrix **C** describes charge−charge interactions. Solving these linear equations is identical to variational minimization of the classical energy for a collection of interacting atoms described by their atomic polarizability and capacitance, under the constraint that the total charge of the system is fixed using the Lagrangian multiplier, λ.[38]

To obtain molecular response properties, we will use linear response theory to obtain the first-order change in the density due to a time-dependent perturbation. We will use the typical convention and identify indices a and b with virtual orbitals, i and j with occupied orbitals, and s and t with general orbitals. The first-order change in the density is

$$\rho'(\mathbf{r},\omega) = \sum_{i,a} P'_{ia}(\omega)\phi_i(\mathbf{r})\phi_a^*(\mathbf{r}) + P'_{ai}(\omega)\phi_a(\mathbf{r})\phi_i^*(\mathbf{r}) \quad (7)$$

in terms of the first-order density matrix ($P'_{st}(\omega)$)

$$P'_{st}(\omega) = \frac{\Delta n_{st}}{\omega - \omega_{st} + i\Gamma} V'^{\text{eff}}_{st}(\omega) \tag{8}$$

where Δn_{st} is the difference in occupation number and Γ is a phenomenological energy broadening term that is due to damping of the excited state; that is, it is related to the effective lifetime of the QM excited state. The change in effective potential $V'^{\text{eff}}_{st}(\omega)$ is given by

$$V'^{\text{eff}}_{st}(\omega) = V'^{\text{pert}}_{st}(\mathbf{r},\omega) + V'^{\text{Coul}}_{st}(\mathbf{r},\omega) + V'^{\text{XC}}_{st}(\mathbf{r},\omega) + V'^{\text{DIM}}_{st}(\mathbf{r},\omega) \tag{9}$$

and is composed of the Coulomb, XC, and DIM potentials, respectively, and V'^{pert}_{st} is the external perturbation given by

$$\hat{V}^{\text{pert}}(\mathbf{r},\omega) = \hat{V}^{\text{ext}}(r_j,\omega) + \hat{V}^{\text{loc}}(r_j,\omega) \tag{10}$$

where $\hat{V}^{\text{ext}}(r_j,\omega)$ represents the applied external potential, and the local field operator ($\hat{V}^{\text{loc}}(r_j,\omega)$) is given as

$$\hat{V}^{\text{loc}}(r_j,\omega) = \sum_m q^{\text{ext}}_m(\omega) T^{(0)}_{jm} + \sum_m \mu^{\text{ext}}_{m,\alpha}(\omega) T^{(1)}_{jm,\alpha} \tag{11}$$

The $q^{\text{ext}}_m(\omega)$ and $\mu^{\text{ext}}_{m,\alpha}(\omega)$ are the charges and dipoles induced in the DIM system due to the external perturbation and are found by solving a set of linear equations similar to what is done for the DIM operator.[41]

The dipole matrix of the QM system, $H^{\alpha}_{st}(\omega)$, is calculated as

$$H^{\alpha}_{st}(\omega) = \langle s|\hat{\mu}_{\alpha} + \hat{V}^{\text{loc}}_{\alpha}(\omega)|t\rangle \tag{12}$$

where $\hat{\mu}_{\alpha}$ is the QM dipole operator in the α direction and $\hat{V}^{\text{loc}}_{\alpha}(\omega)$ is the complex local field operator in the α direction. From the solution of the linear response equations, we get access to excitation energies,[40] frequency-dependent polarizabilities,[41] and recently the frequency-dependent first-hyperpolarizability using the $(2n+1)$ rule.[43]

Two different DIM/QM models are implemented for treating the metal nanoparticle. In the capacitance–polarizability interaction model (CPIM), each atom is described by an atomic polarizability and an atomic capacitance and is well suited for small silver nanoparticle systems (<10 000 atoms).[38,39] Currently, the CPIM model has only been parametrized for small spherical silver nanoparticles but could be extended to other metals. To study large systems, we will use the polarizability interaction model (PIM) model where only an atomic polarizability derived from the experimental bulk dielectric constant is used; this is similar to what is done in the discrete-dipole approximation.[44] Since the nanoparticle is treated atomistically, any shape can be modeled, but so far applications of DIM/QM have only considered quasi-spherical nanoparticles. In PIM, the atomic polarizabilities are derived from the bulk dielectric constant, which is appropriate for nanoparticles with dimensions above 5 nm. For smaller nanoparticles, size corrections due to enhanced electron-surface scattering should be employed as is typical.[45] The computational bottleneck in the DIM/QM method is the solution of the linear equations given in eq 6, which is of the order $3N$ for PIM ($4N+1$ for CPIM) where N is the number of atoms. To solve these linear equations efficiently, we implemented an iterative solver and combined it with a fast matrix–vector multiplication using a multilevel cell–multipole method.[46] Using this approach, we are able to model nanoparticles of large size (~1 000 000 atoms or ~40 nm diameter). Retardation effects are currently not included in the DIM/QM model, which limits the size of the nanoparticles that can be studied to roughly 1/10th of the wavelength of the incident light. Finally, solvent effects are also neglected in the current implementation; however, such effects could be included by embedding the total system in a continuum dielectric matrix or by explicitly including solvent molecules in a QM/MM model. These effects will be important for direct comparison with experiments since the effects of the surrounding matrix is known to affect the plasmon position and field enhancements.[28,47]

3. Molecule–Metal Interactions within the DIM/QM Method

In the DIM/QM method, the interactions between the molecule and the metal surface are described in terms of two distinct mechanisms. The first mechanism involves the interactions between the molecular charge distribution and the metal surface, which is accounted for self-consistently through the $\hat{V}^{\text{DIM}}(\omega)$ operator. The interaction can be thought of as an image field effect or a solvation effect due to the interactions between the molecule and the metal polarizability. The interactions with the metal surface lead to a polarization of both the ground state density and the induced density of the molecule, which affects both ground state properties and excited state properties. The second mechanism involves the polarization induced into the metal nanoparticle due to the interactions with the external field. This is accounted for through the $\hat{V}^{\text{loc}}(\omega)$ operator, which describes the enhanced near field due to the plasmon excitation of the metal nanoparticle. One can show that

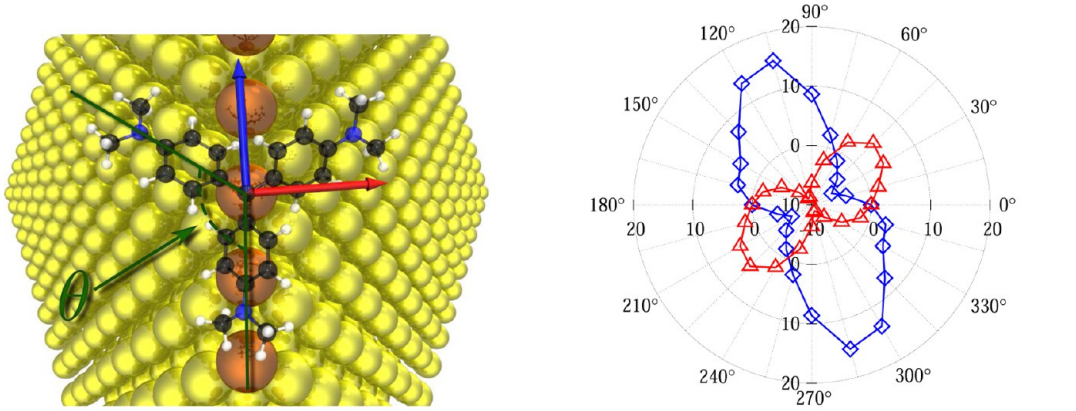

(a) Orientation of CV (b) Shift in excitation energies as a function of θ

FIGURE 1. (a) Orientation of CV on the edge of a Au_{1330} tetrahedral nanoparticle. Transition dipole moment for $S1$ and $S2$ are represented by blue and red arrow, respectively. (b) Polar plot of shift in excitation energy for $S1$ (diamonds) and $S2$ (triangles) of CV as a functions of angle θ. Adapted with permission from ref 40.

the effective molecular properties calculated using DIM/QM contains both the response induced in the molecule due to the metal nanoparticle and the response of the metal nanoparticle induced by the molecule. In the following, we will briefly illustrate the importance of both mechanisms in describing the response properties of molecules interacting with a metal nanoparticle.

3.1. Importance of Image Field Effects. Both SERS on resonance with a molecular excitation (SERRS) and exciton−plasmon hybridization depend strongly on spectral overlap between the plasmon excitation and the molecular resonance. For such systems, it is crucial to understand how the metal nanoparticle influences the molecular excitations. We have shown that the excitation energy depends strongly on the local environment of the metal nanoparticle.[40] This is illustrated in Figure 1 where we plot the orientation dependence for the two lowest excitation energies of crystal violet (CV) relative to a Au_{1330} tetrahedral nanoparticle. Only the image field effects were included in these simulations. The image field interactions were shown to break the degeneracy of the lowest excitation found at 542 nm in the gas phase, red-shifting the $S1$ transition to be at 585 nm and blue-shifting the $S2$ state to be at 534 nm. We find that the image field effects are comparable to those due to solvation and are in good agreement with the experimental absorption spectra in solution where the two states are found at 587 and 539 nm, respectively.[48] We also find that the excitation energies depend strongly on the orientation of the molecule near the metal surface. Orientations where the transition dipole moment is aligned with the edge of the nanoparticle lead to shifts of up to 15 nm. One rationale for this is that in this orientation the transition dipole couples strongly to its image due to a larger electric field near the edge. Such variation in the excitation energies due to the local environment is important for understanding single-molecule experiments based on SERRS. While the variation in excitation energies will average out in ensemble measurements, single-molecule experiments will be sensitive to the fluctuations of the excitation energies. Single-molecule SERS occurs predominantly from electromagnetic hotspots in the junction between nanoparticles that typically are only a few nanometers in dimensions. Detuning from resonance by 10−20 nm could lead to variations in the SERRS intensities resulting in intensity fluctuations due to movement of the molecules in the hotspot. Our results indicate that the specific orientation of the molecule within the hotspot will also influence the total Raman cross section.

3.2. Importance of Local Field Effects. The above results illustrate the influence of the local environment of a metal nanoparticle on the excitation energies of a molecule; however, the simulations did not include the local field effects. To include the local field effects, we simulated the molecular absorption of a substituted naphthoquinone interacting with a Ag_{2057} nanoparticle.[41] The system was chosen so that the molecule absorption band overlapped with the plasmon excitation. In Figure 2, we plot the molecular absorption for two different orientations of the molecule relative to the metal nanoparticle as a function of distance from the surface. The main difference between the two orientations is the direction of the transition dipole moment of $S1$ as indicated in Figure 2. For the FLAT orientation, this leads to destructive interference with the induced polarization in the metal nanoparticle and thus a reduction in the molecular absorption. In the SIDE orientation,

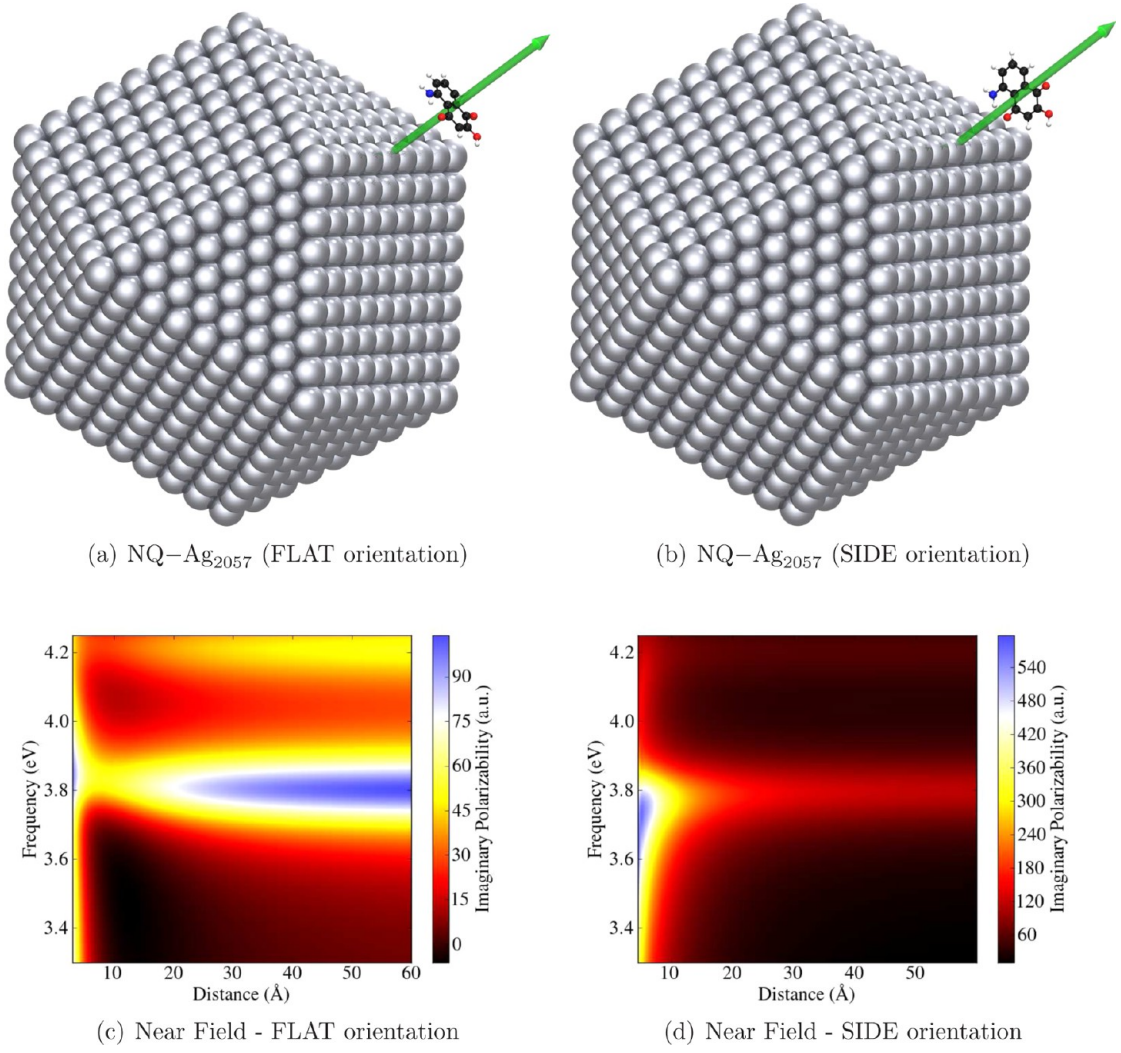

FIGURE 2. The NQ−Ag_{2057} system (a) in the FLAT orientation and (b) in the SIDE orientation. Frequency-dependent imaginary polarizability ($^{I}(\omega)$) as a function of distance and frequency for the NQ−Ag_{2057} system for the (c) FLAT orientation and (d) SIDE orientation. Adapted with permission from ref 41.

*S*1 points toward the metal nanoparticle, and this leads to constructive interference with the metal nanoparticle's induced polarization and a significant increase in the molecular absorption. This can be thought of as an interference effect between the molecular transition dipole moment and the plasmon excitation similar to that observed in surface-enhanced fluorescence.[29,49] Alternatively, this can be understood by considering the molecule and nanoparticle as two interacting point polarizable objects.[41] The imaginary polarizability of the total interacting system can be approximated as

$$\alpha_{\perp}^{I} = \alpha_{M}^{I} + \alpha_{NP}^{I} - \frac{2(\alpha_{M}^{R}\alpha_{NP}^{I} + \alpha_{M}^{I}\alpha_{NP}^{R})}{r^{3}} \quad (13)$$

$$\alpha_{\parallel}^{I} = \alpha_{M}^{I} + \alpha_{NP}^{I} + \frac{4(\alpha_{M}^{R}\alpha_{NP}^{I} + \alpha_{M}^{I}\alpha_{NP}^{R})}{r^{3}} \quad (14)$$

where α_M is the polarizability of the molecule, α_{NP} the polarizability of the metal nanoparticle, and r is center-to-center distance. Superscript R and I refers to the real and imaginary part of the polarizability, respectively. For the FLAT orientation, the largest component of the polarizability is perpendicular to the separation axis, whereas the opposite is true for the SIDE orientation. This shows that the interactions between the real polarizability component of one system with the imaginary polarizability component of the other system governs the coupling between the two systems in agreement with experimental observations.[50,51] This leads to a large increase in the molecular absorption when the transition dipole moment of an excitation is oriented toward the metal nanoparticle. For the case with the transition dipole moment oriented perpendicular to the metal nanoparticle the molecular absorption is reduced. Thus, the molecular absorption can be engineered by controlling both the distance and the

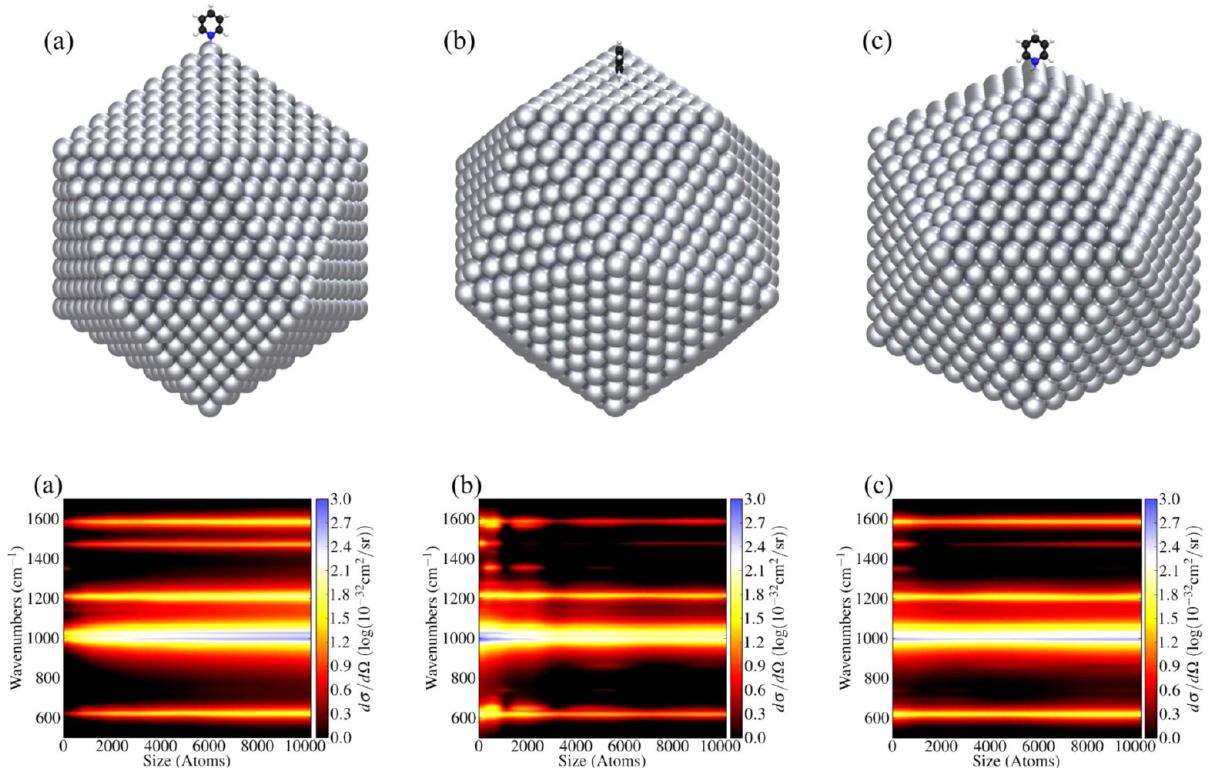

FIGURE 3. Upper figures represent the different pyridine adsorption sites of an icosahedral Ag_{2057} nanoparticle, (a) vertex, (b) face, and (c) edge. Lower figures display the Raman differential cross section of pyridine at three adsorption sites, (a) vertex, (b) face, and (c) edge, as function of the icosahedral nanoparticle's size. Adapted with permission from ref 42.

orientation of the molecule relative to the metal nanoparticle. This is of great importance for plasmon hybridization, plasmon enhanced photochemistry, and SERRS, which rely on overlap between the molecular resonance and the plasmon excitation.

4. Describing SERS Using DIM/QM

Since the DIM/QM method retains an atomistic description of the metal nanoparticle, it is uniquely suited for understanding the influence of the local environment on the SERS spectra. An important feature of the DIM/QM model is that the changes in the molecular geometry due to adsorption onto the metal nanoparticle are described by optimizing the molecular geometry.[42] Below, we will present simulations of the SERS spectrum of pyridine using DIM/QM. Pyridine is a standard model system for understanding SERS. We will focus on the importance of the local environment, distance from the surface, and the size of the metal nanoparticle. We will also present a comparison between enhancement factors obtained using DIM/QM and contrast that against the traditional $|E|^4$ approximation.

4.1. Adsorption Site Dependence. To understand the influence of the local environment on SERS, we initially simulated the spectrum of pyridine at three different adsorption sites on a small silver metal nanoparticle. In Figure 3, we plot the Raman spectra of pyridine as a function of the nanoparticle's size for the three different adsorption sites. The icosahedral nanoparticles studied in this work are characterized by a strong and very broad (i.e., the full width at half-maximum is ~1 eV) absorption band around 3.7 eV due to the plasmon excitation. The broad plasmon excitation is a result of increased surface scattering due to the small size of the nanoparticle.[39] The enhancement factors based on the local fields are between a factor of 10 and 100, in good agreement with the observed enhancements of the Raman spectra presented in Figure 3. The largest field enhancements are found around $\omega = 3.0$ eV, which do not correlate with the maximum of the plasmon excitation. This is typical of broad plasmon peaks and has, for example, been found experimentally for SERS of Pt nanoparticles.[52] The Raman spectra obtained from the three different adsorption sites show a distinct dependence on the size of the metal nanoparticle. For the vertex site, we find an increase in the Raman scattering with increasing size of the nanoparticle. This is expected due to the increased local electric fields at a sharp point like the vertex. We find the

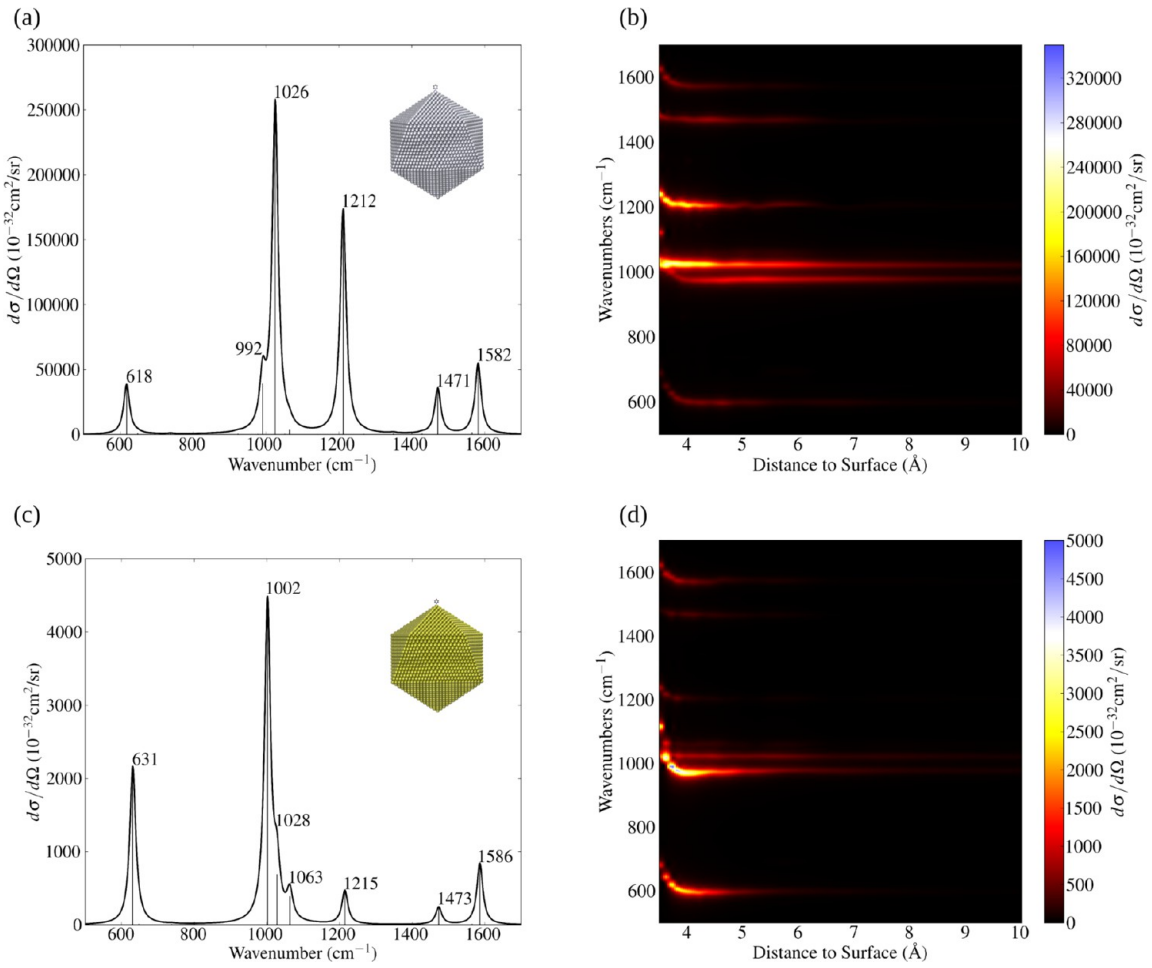

FIGURE 4. SERS spectra of pyridine adsorbed on the vertex of a Ag_{10179} or Au_{10179} icosahedral nanoparticle. (a) SERS spectrum on Ag nanoparticle at the equilibrium geometry, (b) SERS spectrum on Ag nanoparticle as a function of distance between the center of mass of pyridine and metal surface, (c) SERS spectrum on Au nanoparticle at the equilibrium geometry, and (d) SERS spectrum on Au nanoparticle as a function of distance between the center of mass of pyridine and metal surface.

opposite behavior for the face site, which shows the largest enhancements for the smallest nanoparticles. One explanation for this is that for small nanoparticles, the molecules sit in the vicinity of three vertices that all have strong electric fields. As the nanoparticle size increases, the vertices move away from the molecule and the local geometry resembles that of a flat metal surface, which does not support strong local fields. This illustrates that the Raman scattering from a metal nanoparticle likely comes only from a small set of adsorption sites with high local electric fields associated with them. All the results indicate a strong dependence on the nanoparticle's local environment for the Raman spectra and highlight the importance of an atomistic description of the system.

4.2. Distance Dependence. In Figure 4, we plot the SERS spectra of pyridine adsorbed on the vertex of Ag_{10179} and Au_{10179} icosahedral nanoparticles. We also plot the Raman spectra as a function of the distance from the surface. The incident frequencies for computations of the Raman cross sections were set to match the plasmon excitation for the silver and gold icosahedral nanoparticles of 3.60 eV (344 nm) and 2.46 eV (504 nm), respectively. We see that the enhancements are significantly larger for silver than for gold due to the more free electron nature of silver. The SERS spectrum for distances 6 Å away from the surface is dominated by the two ring breathing modes around 1000 cm^{-1}. As the distance is reduced, several additional modes get enhanced, especially the mode at 1212 cm^{-1} for pyridine on the silver nanoparticle. The mode at 1212 cm^{-1} is often associated with the CM since experiments have shown that it depends strongly on the electrode potential in SERS measurements on roughened Ag electrodes.[53] Interestingly, we still see that this mode is strong in the SERS spectrum even though the DIM/QM method does not account for

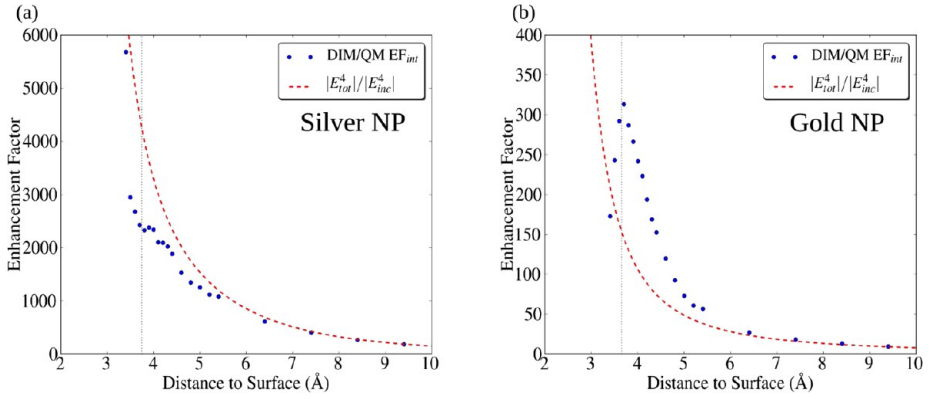

FIGURE 5. Average enhancement factors of pyridine on a Ag_{10179} (a) or Au_{10179} (b) icosahedral nanoparticle as a function of the distance between the center of mass of pyridine and metal surface. Vertical lines indicate the equilibrium bonding distance. Dots indicate DIM/QM results and dashed line indicates $|E|^4$ enhancements calculated at the center of mass of the pyridine molecule.

CM in its present form. DIM/QM does include the geometric changes in the molecule when adsorbed onto the metal surface, which does lead to a change in the Raman spectrum. For distances below 4 Å, we see that the vibrational frequencies change significantly due to a distortion of the pyridine ring when adsorbed onto the metal surface.

To quantify the distance dependence of the SERS enhancement, we calculated the average enhancement factors[19] as $EF_{int} = \Sigma_k(I^k_{adsorbed}(\omega)/I^k_{free}(\omega))$, where $I^k_{adsorbed}(\omega)$ and $I^k_{free}(\omega)$ are the intensities of the kth normal mode of pyridine adsorbed to the metal nanoparticle and for the free molecule, respectively. In Figure 5, we plot the average enhancement factors as a function of distance from the surface. We also include the enhancement factors calculated using the $|E|^4$ approximation for comparison. Here, the electric field enhancements were evaluated at the center of mass of the pyridine molecule. We see that there is good agreement between the two enhancement factors once the distance is longer than 6 Å. For short distances, there is a significant difference between the enhancements based on the local field and those actually calculated. The $|E|^4$ approximation significantly overestimates the enhancements for silver, whereas for gold it underestimates them. This is most likely because in DIM/QM the molecule is interacting with the complete inhomogeneous electric field, which varies over the dimensions of the molecule. As the distance is increased, the molecule sits at the tail of the field, which is more homogeneous, and thus the field calculated at the center of mass is a good representation of the actual field felt by the molecule. This clearly demonstrates the importance of accounting for the field variation over the dimension of the molecule when simulating the SERS spectrum. We also see that around the equilibrium distance, the DIM/QM enhancement actually decreases. This is especially clear for pyridine on the gold nanoparticle. The reason for this decrease is that the field at the surface of the metal nanoparticle is reduced once the charge distribution of the molecule overlaps with the charge distribution of the metal atoms. This is a quantum mechanical effect that is approximated in DIM/QM by screening the interactions between the molecule and the metal nanoparticle at short distances.

4.3. Size Dependence. To understand the size dependence of the SERS enhancement, we calculated the enhancements for the two ring breathing modes at 996 and 1026 cm^{-1} for pyridine on the vertex of a silver nanoparticle. Nanoparticles with a radius from 4 to 20 nm were considered. The largest nanoparticles contained about 1 million atoms illustrating that DIM/QM can calculate the SERS spectra of molecules interacting with realistic sized metal nanoparticles. The enhancements for the two modes are plotted in Figure 6 as a function of size of the metal nanoparticle. The enhancements calculated using the local field at the center of mass of pyridine is included for comparison. We see that the enhancements increase from about 10^3 at a radius of 4 nm to about 10^6 at a radius of 20 nm for both modes. The agreement with the enhancements calculated using the $|E|^4$ approximation is excellent once a mode dependent scale factor has been included. For the mode at 996 cm^{-1}, a scale factor of 0.15 was used whereas only a scale factor of 0.55 was needed for the mode at 1026 cm^{-1}. Thus, the enhancements approximated by the local fields are found to significantly overestimate the calculated enhancements, even though the local field was evaluated at the center of mass of the pyridine and not the nitrogen atom binding to the metal surface. This again illustrates that the enhancement mechanism in DIM/QM is

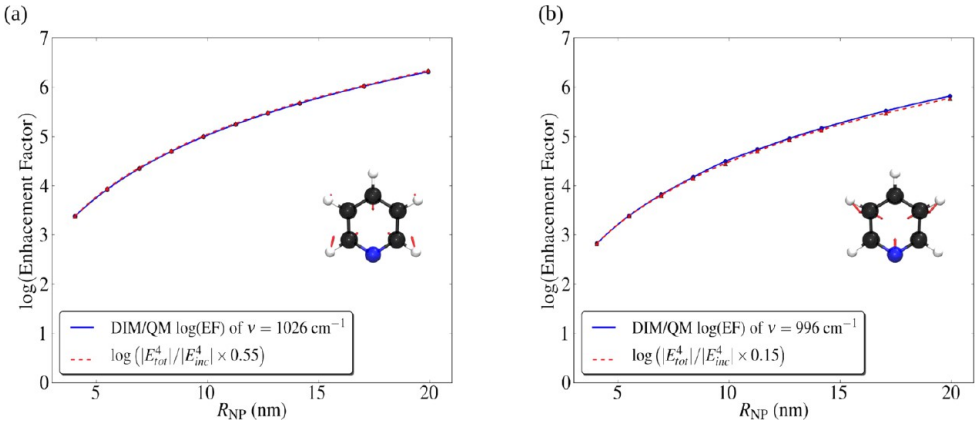

FIGURE 6. The enhancement factors for the two ring breathing modes of pyridine on an icosahedral nanoparticle as a function of the size of the metal nanoparticle: (a) the 1026 cm^{-1} mode and (b) the 996 cm^{-1} mode. Also, included is the scaled enhancements predicted using the local fields calculated at the center of mass of the pyridine.

electromagnetic in nature and that the field felt by the molecule is inhomogeneous and thus different for each vibrational mode. Our results seem to indicate that the $|E|^4$ enhancement mechanism is accurate to within an order of magnitude, highlighting its approximate nature. This is important since disagreements within an order of magnitude between experimentally measured enhancements and those obtained from simulations is often attributed to the CM. Here we show that the difference need not be due to the CM but could be due to the approximation of using $|E|^4$ enhancement estimates.

5. Conclusion

In this Account, we have discussed our recent work using the DIM/QM method for simulating the optical properties, especially SERS, of molecules interacting with plasmonic metal nanoparticles. DIM/QM is a hybrid method that consists of an atomistic electrodynamics model of the metal nanoparticle and a TDDFT description of the molecule. In contrast to most previous work, this enables us to retain the detailed atomistic structure of the nanoparticle and provides a natural bridge between the electronic structure methods and the macroscopic electrodynamics description. Using the DIM/QM method, we have examined in detail the importance of the local environment on molecular excitation energies, enhanced molecular absorption, and SERS. Applications of DIM/QM to understanding plasmonic effects on molecular excitation energies, absorption, and SERS have been discussed. We have shown that the local environment of the metal nanoparticle, the distance from the surface, and the relative orientation plays an important role in determining the molecular response properties. To test the standard practice of computing SERS enhancements as $|E|^4$, we presented a direct comparison with enhancements obtained using DIM/QM. Close to the metal surface, we find significant difference between the predicted enhancements and those obtained using DIM/QM; however, as the distance is increased the enhancements agree perfectly. The reason for this is that in DIM/QM, the molecule is perturbed by the complete inhomogeneous electric field, which varies over the dimensions of the molecule. This was also reflected by DIM/QM showing mode dependent enhancements in contrast to the simple $|E|^4$ approximation. Our results highlight the importance of explicitly considering the specific local environment and directly simulating the SERS spectra to understand the molecule–plasmon coupling. Future challenges will be to treat a small portion of the metal nanoparticle quantum mechanically so that charge transfer between molecule and metal can be described. Also, the DIM/QM method should be extended to include solvent effects.

6. Computational Methods

All computations were performed with a local developmental version of the Amsterdam Density Functional (ADF) software package with the DIM/QM method implemented. All geometries, vibrational frequencies, numerical polarizability derivatives, Raman cross section, and Raman enhancement factors were computed with the BP86 functional and a triple ζ polarized basis set (TZP). Pyridine was adsorbed via the lone pair of nitrogen to a vertex site of the nanoparticle. The structures were fully optimized except for the distance dependence study where a single constraint was added to the metal–nitrogen bond length. The nanoparticles were constructed as icosahedrons with the metal–metal bond length set to experimental distances of 2.889 Å for silver and 2.884 Å for gold. The PIM parameters for silver and gold radii

were set to the experimental radii of 1.4445 and 1.442 Å, respectively, while the required frequency dependent parameters were computed from the experimental Johnson and Christy dielectric functions.[54] The frequency dependent polarizability lifetime (Γ) was set to 0.10 eV.

The purely classical part of the DIM/QM force field was computed as previously reported[42] with the addition of the gold coordination dependent parameters as $CN_{max} = 12.0$, $|r_{min}| = 3.0$ Å, $|r_{max}| = 5.0$ Å, $\varepsilon_0 = 3.765$ kcal/mol, $\varepsilon_1 = 1.506$ kcal/mol, $r_0 = 1.659$ Å, and $r_1 = 1.864$ Å. The gold coordination dependent parameters were optimized in a similar manner to the silver set previously reported.[42] For the distance dependence study, we found the cutoff for the nitrogen chemisorption correction introduced a noncontinuous potential energy surface (PES). To have a smooth PES for the distance dependence study, the cutoff was removed from the nitrogen chemisorption correction. To account for this, the nitrogen parameter was adjusted to $\varepsilon_1 = 6.275$ kcal/mol.

For the size dependence study, we found that the geometric structure and vibrational modes of the adsorbed pyridine had negligible changes as the size of the nanoparticle increases. We chose to use the vibrational displacement vectors of an adsorbed pyridine on the 10179 atom ($R_{NP} = 4.0$ nm) nanoparticle for the computation of the numerical polarizability derivatives for all larger nanoparticles.

L.J. acknowledges the CAREER program of the National Science Foundation (Grant No. CHE-0955689) for financial support, start-up funds from the Pennsylvania State University, and support received from Research Computing and Cyberinfrastructure, a unit of Information Technology Services at Penn State. S.M.M. acknowledges the Academic Computing Fellowship from the Pennsylvania State University Graduate School.

BIOGRAPHICAL INFORMATION

John L. Payton received a Ph.D. in Chemistry at Case Western Reserve University in 2010 and was a Postdoctoral researcher in the Jensen group until 2012.

Seth M. Morton received a Ph.D. in chemistry at the Pennsylvania State University in 2012 doing research in the Jensen group.

Justin E. Moore received a B.S. in chemistry at West Virginia University in 2010 and is a graduate student in the Jensen group.

Lasse Jensen received a Ph.D. in chemistry at Rijksuniversiteit Groningen, The Netherlands, in 2004 and is an Associate Professor at the Pennsylvania State University.

FOOTNOTES

*To whom correspondence should be addressed. E-mail: jensen@chem.psu.edu.
The authors declare no competing financial interest.

REFERENCES

1 Willets, K. A.; Van Duyne, R. P. Localized Surface Plasmon Resonance Spectroscopy and Sensing. *Annu. Rev. Phys. Chem.* **2007**, *58*, 267–297.
2 Myers Kelley, A. Hyper-Raman Spectroscopy by Molecular Vibrations. *Annu. Rev. Phys. Chem.* **2010**, *61*, 41.
3 Barnes, W. L. Fluorescence near Interfaces: The Role of Photonic Mode Density. *J. Mod. Opt.* **1998**, *45*, 661–699.
4 Lakowicz, J. R. Radiative Decay Engineering: Biophysical and Biomedical Applications. *Anal. Biochem.* **2001**, *298*, 1–24.
5 Halas, N. J.; Lal, S.; Chang, W.-S.; Link, S.; Nordlander, P. Plasmons in Strongly Coupled Metallic Nanostructures. *Chem. Rev.* **2011**, *111*, 3913–3961.
6 Anker, J. N.; Hall, W. P.; Lyandres, O.; Shah, N. C.; Zhao, J.; Van Duyne, R. P. Biosensing with Plasmonic Nanosensors. *Nat. Mater.* **2008**, *7*, 442–453.
7 Moskovits, M. Surface-Enhanced Spectroscopy. *Rev. Mod. Phys.* **1985**, *57*, 783–826.
8 Campion, A.; Kambhampati, P. Surface-Enhanced Raman Scattering. *Chem. Soc. Rev.* **1998**, *27*, 241.
9 Kneipp, K.; Kneipp, H.; Itzkan, I.; Dasari, R. R.; Feld, M. S. Ultrasensitive Chemical Analysis by Raman Spectroscopy. *Chem. Rev.* **1999**, *99*, 2957–2976.
10 Link, S.; El-Sayed, M. A. Optical Properties and Ultrafast Dynamics of Metallic Nanocrystals. *Annu. Rev. Phys. Chem.* **2003**, *54*, 331–366.
11 Michaels, A. M.; Nirmal, M.; Brus, L. E. Surface-Enhanced Raman Spectroscopy of Individual Rhodamine 6G Molecules on Large Ag Nanocrystals. *J. Am. Chem. Soc.* **1999**, *121*, 9932–9939.
12 Xu, H.; Bjerneld, E. J.; Käll, M.; Börjesson, L. Spectroscopy of Single Hemoglobin Molecules by Surface Enhanced Raman Scattering. *Phys. Rev. Lett.* **1999**, *83*, 4357–4360.
13 Dieringer, J. A.; Lettan, R. B.; Scheidt, K. A.; Van Duyne, R. P. A Frequency Domain Existence Proof of Single-Molecule Surface-Enhanced Raman Spectroscopy. *J. Am. Chem. Soc.* **2007**, *129*, 16249–16256.
14 Kneipp, K.; Wang, Y.; Kneipp, H.; Perelman, L. T.; Itzkan, I.; Dasari, R. R.; Feld, M. S. Single Molecule Detection Using Surface-Enhanced Raman Scattering (SERS). *Phys. Rev. Lett.* **1997**, *78*, 1667–1670.
15 Nie, S. M.; Emory, S. R. Proping Single Molecules and Single Nanoparticles by Surface-Enhanced Raman Scattering. *Science* **1997**, *275*, 1102–1106.
16 Gersten, J.; Nitzan, A. Electromagnetic Theory of Enhanced Raman Scattering by Molecules Adsorbed on Rough Surfaces. *J. Chem. Phys.* **1980**, *73*, 3023–3037.
17 Le Ru, E. C.; Etchegoin, P. G. Rigorous Justification of the $|E|^4$ Enhancement Factor in Surface Enhanced Raman Spectroscopy. *Chem. Phys. Lett.* **2006**, *423*, 63–66.
18 Jensen, L.; Aikens, C. M.; Schatz, G. C. Electronic Structure Methods for Studying Surface-Enhanced Raman Scattering. *Chem. Soc. Rev.* **2008**, *37*, 1061–1073.
19 Morton, S. M.; Jensen, L. Understanding the Molecule−Surface Chemical Coupling in SERS. *J. Am. Chem. Soc.* **2009**, *131*, 4090–4098.
20 Morton, S. M.; Silverstein, D. W.; Jensen, L. Theoretical Studies of Plasmonics using Electronic Structure Methods. *Chem. Rev.* **2011**, *111*, 3962–3994.
21 Moore, J. E.; Morton, S. M.; Jensen, L. Importance of Correctly Describing Charge-Transfer Excitations for Understanding the Chemical Effect in SERS. *J. Phys. Chem. Lett.* **2012**, *3*, 2470–2475.
22 Saikin, S. K.; Chu, Y.; Rappoport, D.; Crozier, K. B.; Aspuru-Guzik, A. Separation of Electromagnetic and Chemical Contributions to Surface-Enhanced Raman Spectra on Nanoengineered Plasmonic Substrates. *J. Phys. Chem. Lett.* **2010**, *1*, 2740–2746.
23 Zhao, J.; Pinchuk, A. O.; McMahon, J. M.; Li, S.; Ausman, L. K.; Atkinson, A. L.; Schatz, G. C. Methods for Describing the Electromagnetic Properties of Silver and Gold Nanoparticles. *Acc. Chem. Res.* **2008**, *41*, 1710–1720.
24 Savage, K. J.; Hawkeye, M. M.; Esteban, R.; Borisov, A. G.; Aizpurua, J.; Baumberg, J. J. Revealing the Quantum Regime in Tunnelling Plasmonics. *Nature* **2012**, *491*, 574–577.
25 Zhao, L. L.; Jensen, L.; Schatz, G. C. Pyridine-Ag_{20} Cluster: A Model System for Studying Surface Enhanced Raman Scattering. *J. Am. Chem. Soc.* **2006**, *128*, 2911–2919.
26 Corni, S.; Tomasi, J. Enhanced Response Properties of a Chromophore Physisorbed on a Metal Particle. *J. Chem. Phys.* **2001**, *114*, 3739–3751.
27 Corni, S.; Tomasi, J. Excitation Energies of a Molecule Close to a Metal Surface. *J. Chem. Phys.* **2002**, *117*, 7266–7278.
28 Corni, S.; Tomasi, J. Surface Enhanced Raman Scattering from a Single Molecule Adsorbed on a Metal Particle Aggregate: A Theoretical Study. *J. Chem. Phys.* **2002**, *116*, 1156–1164.
29 Vukovic, S.; Corni, S.; Mennucci, B. Fluorescence Enhancement of Chromophores Close to Metal Nanoparticles. Optimal Setup Revealed by the Polarizable Continuum Model. *J. Phys. Chem. C* **2009**, *113*, 121–133.
30 Jørgensen, S.; Ratner, M. A.; Mikkelsen, K. V. Heterogeneous Solvation: An ab Initio Approach. *J. Chem. Phys.* **2001**, *115*, 3792–3803.

31 Neuhauser, D.; Lopata, K. Molecular Nanopolaritonics: Cross Manipulation of near-Field Plasmons and Molecules. I. Theory and Application to Junction Control. *J. Chem. Phys.* **2007**, *127*, No. 154715.

32 Lopata, K.; Neuhauser, D. Multiscale Maxwell-Schrödinger Modeling: A Split Field Finite-Difference Time-Domain Approach to Molecular Nanopolaritonics. *J. Chem. Phys.* **2009**, *130*, No. 104707.

33 Arcisauskaite, V.; Kongsted, J.; Hansen, T.; Mikkelsen, K. V. Charge Transfer Excitation Energies in Pyridine-Silver Complexes Studied by a QM/MM Method. *Chem. Phys. Lett.* **2009**, *470*, 285–288.

34 Masiello, D. J.; Schatz, G. C. Many-Body Theory of Surface-Enhanced Raman Scattering. *Phys. Rev. A* **2008**, *78*, No. 042505.

35 Masiello, D. J.; Schatz, G. C. On the Linear Response and Scattering of an Interacting Molecule-Metal System. *J. Chem. Phys.* **2010**, *132*, No. 064102.

36 Chen, H.; McMahon, J. M.; Ratner, M. A.; Schatz, G. C. Classical Electrodynamics Coupled to Quantum Mechanics for Calculation of Molecular Optical Properties: a RT-TDDFT/FDTD Approach. *J. Phys. Chem. C* **2010**, *114*, 14384–14392.

37 Watson, M. A.; Rappoport, D.; Lee, E. M. Y.; Olivares-Amaya, R.; Aspuru-Guzik, A. Electronic Structure Calculations in Arbitrary Electrostatic Environments. *J. Chem. Phys.* **2012**, *136*, No. 024101.

38 Jensen, L. L.; Jensen, L. Electrostatic Interaction Model for the Calculation of the Polarizability of Large Noble Metal Nanoclusters. *J. Phys. Chem. C* **2008**, *112*, 15697–15703.

39 Jensen, L. L.; Jensen, L. Atomistic Electrodynamics Model for Optical Properties of Silver Nanoclusters. *J. Phys. Chem. C* **2009**, *113*, 15182–15190.

40 Morton, S. M.; Jensen, L. A Discrete Interaction Model/Quantum Mechanical Method for Describing Response Properties of Molecules Adsorbed on Metal Nanoparticles. *J. Chem. Phys.* **2010**, *133*, No. 074103.

41 Morton, S. M.; Jensen, L. A Discrete Interaction Model/Quantum Mechanical Method to Describe the Interaction of Metal Nanoparticles and Molecular Absorption. *J. Chem. Phys.* **2011**, *135*, No. 134103.

42 Payton, J. L.; Morton, S. M.; Moore, J. E.; Jensen, L. A Discrete Interaction Model/Quantum Mechanical Method for Simulating Surface-Enhanced Raman Spectroscopy. *J. Chem. Phys.* **2012**, *136*, No. 214103.

43 Rinaldi, J. M.; Morton, S. M.; Jensen, L. A Discrete Interaction Model/Quantum Mechanical Method for Simulating Nonlinear Optical Properties of Molecules near Metal Surfaces. *Mol. Phys.* **2013**, *111*, 1322–1331.

44 Draine, B. T.; Flatau, P. J. Discrete-Dipole Approximation for Scattering Calculations. *J. Opt. Soc. Am. A* **1994**, *11*, 1491–1499.

45 Coronado, E. A.; Schatz, G. C. Surface Plasmon Broadening for Arbitrary Shape Nanoparticles: A Geometrical Probability Approach. *J. Chem. Phys.* **2003**, *119*, 3926–3934.

46 Kutteh, R.; Nicholas, J. B. Efficient Dipole Iteration in Polarizable Charged Systems Using the Cell Multipole Method and Application to Polarizable Water. *Comput. Phys. Commun.* **1995**, *86*, 227–235.

47 Kelly, K. L.; Coronado, E. A.; Zhao, L. L.; Schatz, G. C. The Optical Properties of Metal Nanoparticles: The Influence of Size, Shape, And Dielectric Environment. *J. Phys. Chem. B* **2003**, *107*, 668–677.

48 Loison, C.; Antoine, R.; Broyer, M.; Dugourd, P.; Guthmuller, J.; Simon, D. Microsolvation Effects on the Optical Properties of Crystal Violet. *Chem.—Eur. J.* **2008**, *14*, 7351–7357.

49 Chance, R. R.; Prock, A.; Silbey, R. In *Advances in Chemical Physics*; Prigogine, I., Rice, S. A., Eds.; John Wiley & Sons, Inc.: Hoboken, NJ, 1978; Vol. 37; Chapter 1, pp 1−65.

50 Zhao, J.; Jensen, L.; Sung, J.; Zou, S.; Schatz, G. C.; Duyne, R. P. V. Interaction of Plasmon and Molecular Resonances for Rhodamine 6G Adsorbed on Silver Nanoparticles. *J. Am. Chem. Soc.* **2007**, *129*, 7647–7656.

51 Juluri, B. K.; Lu, M.; Zheng, Y. B.; Huang, T. J.; Jensen, L. Coupling between Molecular and Plasmonic Resonances: Effect of Molecular Absorbance. *J. Phys. Chem. C* **2009**, *113*, 18499–18503.

52 Hao, Q.; Juluri, B. K.; Zheng, Y. B.; Wang, B.; Chiang, I.-K.; Jensen, L.; Crespi, V.; Eklund, P. C.; Huang, T. J. Effects of Intrinsic Fano Interference on Surface Enhanced Raman Spectroscopy: Comparison between Platinum and Gold. *J. Phys. Chem. C* **2010**, *114*, 18059–18066.

53 Arenas, J. F.; Tocón, I. L.; Otero, J. C.; Marcos, J. I. Charge Transfer Processes in Surface-Enhanced Raman Scattering. Frank-Condon Active Vibrations of Pyridine. *J. Phys. Chem.* **1996**, *100*, 9254–9261.

54 Johnson, P. B.; Christy, R. W. Optical Constants of the Noble Metals. *Phys. Rev. B* **1972**, *6*, 4370–4379.